Electronic Supplementary Material (ESI) for Chemical Communications.

Supporting Information

Phase Transition of Spiropyrans: Impact of Isomerization Dynamics at High Temperatures

Mihael A. Gerkman, Shichen Yuan, Pu Duan, Jennifer Taufan, Klaus Schmidt-Rohr, and Grace G. D. Han*

Department of Chemistry, Brandeis University, 415 South Street, Waltham, MA, 02453, USA

Email: gracehan@brandeis.edu

Methods

^{1}H NMR spectra were recorded in solution on a Varian instrument 400 MHz and internally referenced to tetramethylsilane signal or residual protio-solvent signal. DSC analysis was conducted on a DSC 250 (TA Instruments) with an RSC 90 cooling component. Powder X-ray diffraction (XRD) patterns were recorded on Inel XRG 3000 diffractometer using Cu-Kα radiation (λ = 1.5418 Å) with accelerating voltage and current of 40 kV and 30 mA, respectively. Samples for PXRD were prepared by placing a thin layer of the material on a zero-background silicon crystal plate. Low magnification digital images were acquired using a Celestron Handheld Digital Microscope Pro, and high magnification optical images were obtained by an Olympus BX41 optical microscope with a 100x objective.

Solid-State NMR

Solid-state ^{13}C and ^{1}H NMR experiments were conducted on a BRUKER AVANCE NEO 400 spectrometer in a 4 mm magic angle spinning (MAS) double resonance probe head at 100 MHz and 400 MHz for ^{13}C and ^{1}H, respectively. The ^{13}C chemical shift was referenced to TMS via the carbonyl of α-glycine at 176.49 ppm as a secondary reference. Quantitative multiCP[1] ^{13}C NMR spectra were recorded at MAS frequencies of 14 kHz with signal averaging for 2 to 5 hours, except for the spectrum shown in Fig. 3a, which was measured at 10 kHz with signal averaging for two days. The recycle delay for all the samples was 4 s. The SPINAL-64 supercycle[2] was employed for high-power ^{1}H decoupling during acquisition. MultiCP experiments with recoupled gated decoupling[3] were conducted to select the signals of nonprotonated ^{13}C and mobile CH_3. To check for structural changes in the samples due to the centrifugal force exerted during 14-kHz MAS, multiCP experiments with TOSS[4] were recorded at a low MAS frequency of 3 kHz before and after the 14 kHz measurements. The ACD/C+H NMR predictor was employed to simulate the ^{13}C chemical shifts of the compounds of interest.

UV-Vis Absorption Spectroscopy

UV-Vis adsorption spectra were obtained with a Cary 50 Bio UV-Vis Spectrophotometer in a UV Quartz cuvette with a pathlength of 10 mm. Compounds were dissolved in DMSO (0.01 mg/mL), methanol (0.01 mg/mL), and toluene (0.025 mg/mL). For the MC decay measurement, the UV-Vis absorption was first recorded in the dark for 10 min, then SP samples were irradiated with a UV lamp (365 nm, 100 W) until no change in their absorbance was observed. After the UV lamp was turned off, the samples were monitored in the dark until the original spectra were recovered.

Thin-film samples were prepared by placing powder on a pre-cleaned glass slide and heating up to 210 °C on a hot plate. The melt was sandwiched with another glass slide to spread and fill the entire area. Then it was slowly cooled in 10 °C decrements until room temperature was reached.

The film edges were sealed by LavaLock 650 F High Temp Silicon Adhesive to fix the thickness prior to the UV-Vis measurement on films at various temperatures.

Supporting Note 1. Thermal, NMR, and Optical Analysis of Compound **5**-**8**.

We performed extensive studies of spiropyrans without a nitro group, including unfunctionalized **5**, 6-bromo-functionalized **6**, 6-hydroxy-functionalized **7**, and 8-methoxy-functionalized **8** (Fig. S1a). Upon melting and cooling to -50 °C, compounds **5** and **6** exhibit amorphization, similar to compounds **2** and **3**, while compound **8** shows cold-crystallization after the second heating to 64 °C. Compound **7** decomposes during melting (Fig. S1b).

The analysis of their MC concentration was, however, extremely challenging due to the negligible presence of MC isomers in various organic solutions. Fig. S1c shows NMR spectra of compounds **5**-**8** in MeOH (*i.e.* one of the best solvents) at their maximum concentrations, but the presence of MC isomers is difficult to detect. This is in contrast to compounds **1-4** that show significant MC:SP ratio in MeOH solutions (Fig. S12), which allows us to acquire solution-NMR-calibrated extinction coefficients (Ɛ) of MC **1-4**. Fig. S9c shows an example of compound **2** in a DMSO solution, showing a significant MC concentration of 12% determined by the integration of corresponding NMR peaks. The MC concentration of compound **2** in MeOH is 23%. Since the Ɛ of MC **5-8** could not be obtained, the dopant concentration in their films could not be calculated, either.

Compounds **5**-**8** (T_m of 94-144 °C) decomposed at 180 °C, the initial temperature applied to films **1**-**4** (Fig. 3b) for monitoring MC-to-SP conversion. At temperatures below 150 °C, the absorbance of films **5**-**8** was very low around 500-700 nm and difficult to distinguish from noise (Fig. S1d). Despite the large thickness of films (30-40 μm), the absorbance of MC isomer in the films is very low (< 0.1), compared to compounds **1-4** (see Fig. S10 for 1-5 μm films showing absorbance of 0.5-3.0). Thin films (1-5 μm) of compounds **5-8** did not exhibit any noticeable absorbance at 500-700 nm.

Moreover, compounds **5**-**8** barely photoswitch in toluene or other solvents, so their solution-state MC-to-SP conversion kinetics could not be analyzed, either. These multiple challenges restricted us from directly comparing the dopant levels in compounds **5**-**8** with those of **1-4** presented in the main text.

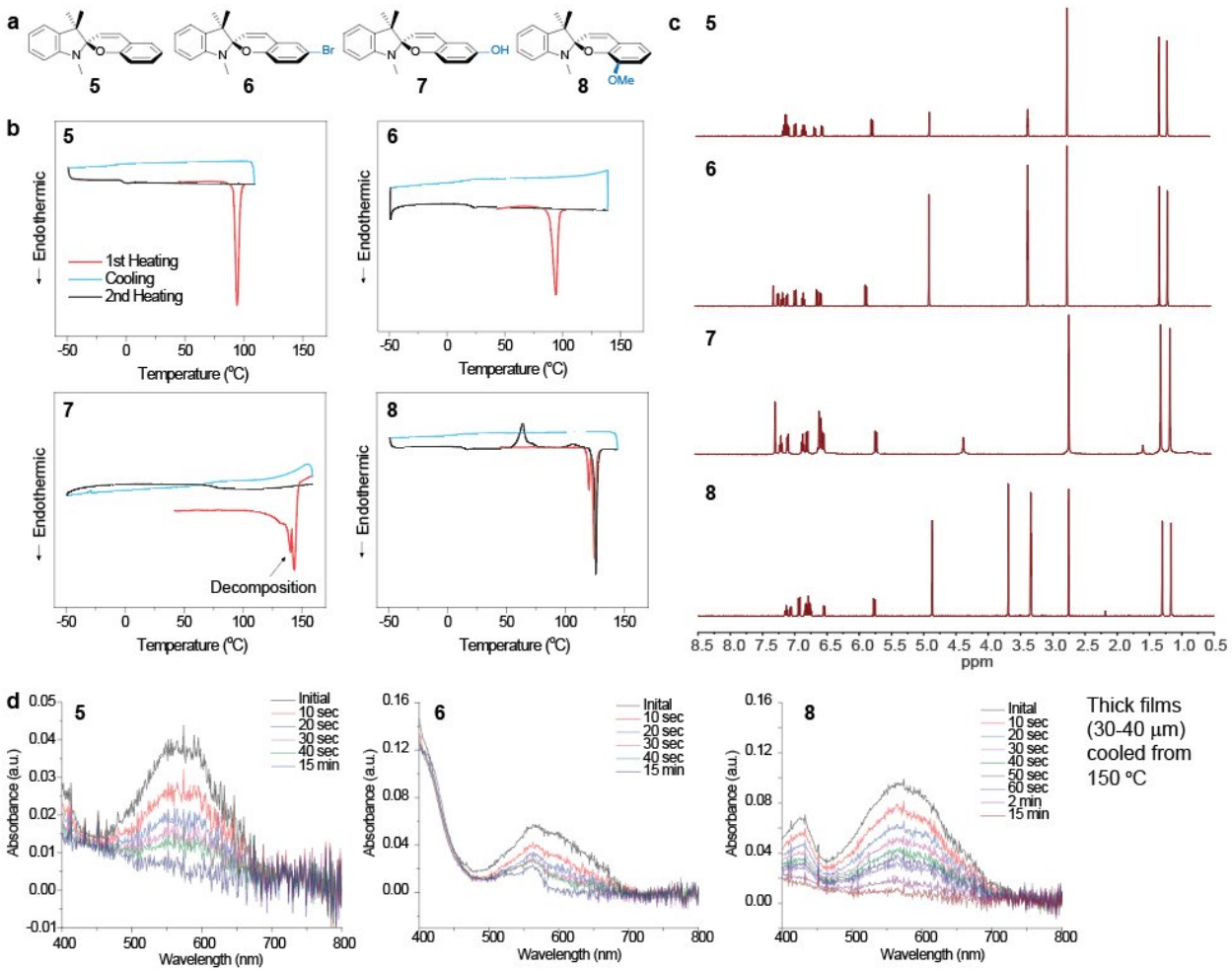

Figure S1. (a) Chemical structures of compounds **5**-**8**. (b) DSC curves of compounds showing initial melting (simultaneous decomposition for compound **7**), cooling to -50 °C, and the second heating. Compounds **5-8** all exhibit lower melting points compared to compounds **1-4**. (c) NMR spectra of compounds **5-8** in concentrated solutions (>1 mg/mL) of MeOH. (d) UV-Vis spectra of compounds **5, 6,** and **8** in thick films (30-40 μm) cooled from 150 °C. Compound **7** is decomposed while melting (not shown).

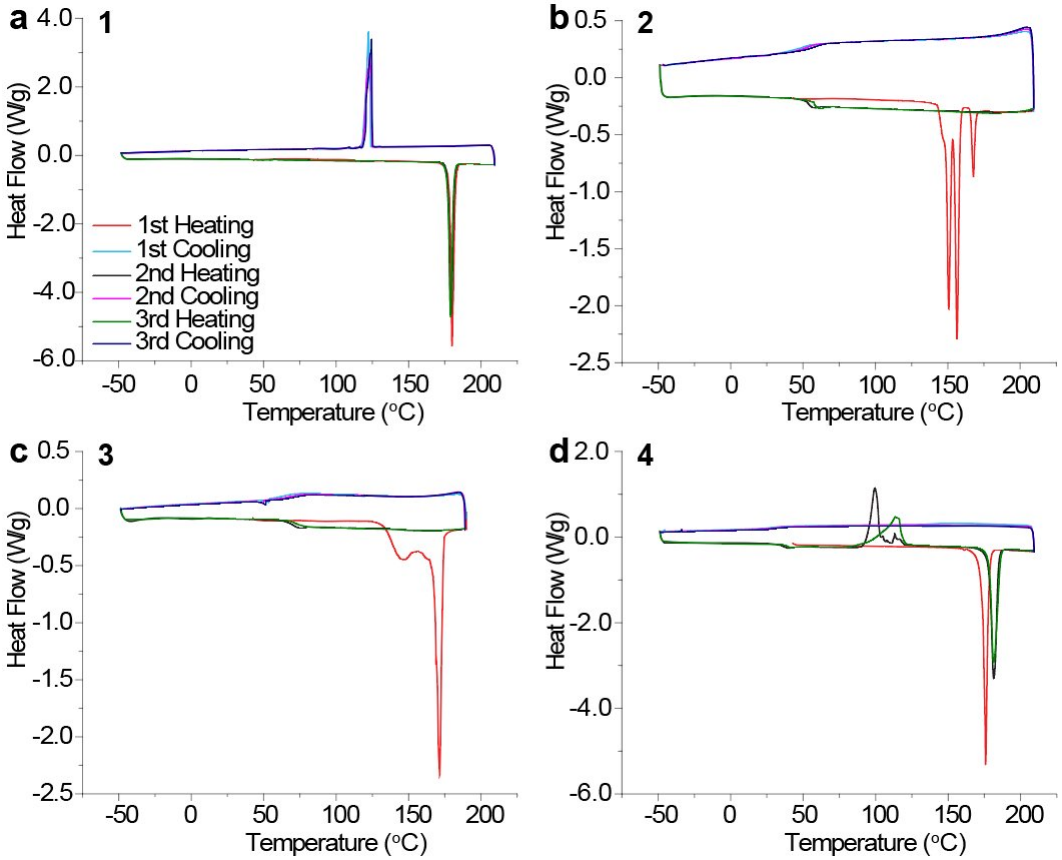

Figure S2. DSC plots of compounds **1**-**4** (a-d) taken during three cycles of heating and cooling. Compound **1**, **2**, and **4** were heated up to 210 °C, and compound **3** was heated up to 180 °C. Compound **1** shows identical melting and crystallization behavior over three cycles. Compounds **2**-**4** exhibits the initial melting of crystalline powder, followed by the amorphization. The subsequent cycles overlap without exothermic features, indicating no sign of thermal decomposition. Cold-crystallization peaks of compound **4** observed on the 2nd and 3rd heating cycles appear within the identical temperature range, but the different shapes indicate the different kinetics of crystallization process.

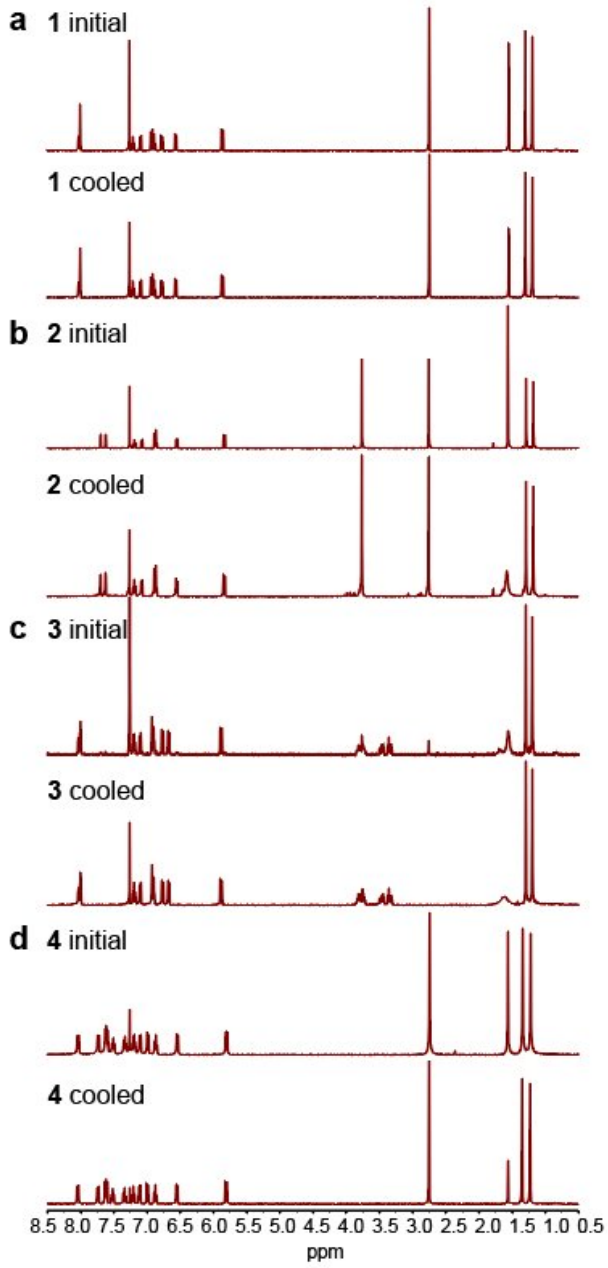

Figure S3. ^{1}H-NMR spectra of compounds **1**-**4** (a-d) taken before (initial crystals) and after three cycles of DSC (cooled; amorphous or crystalline solid) that were performed as shown in Fig. S2.

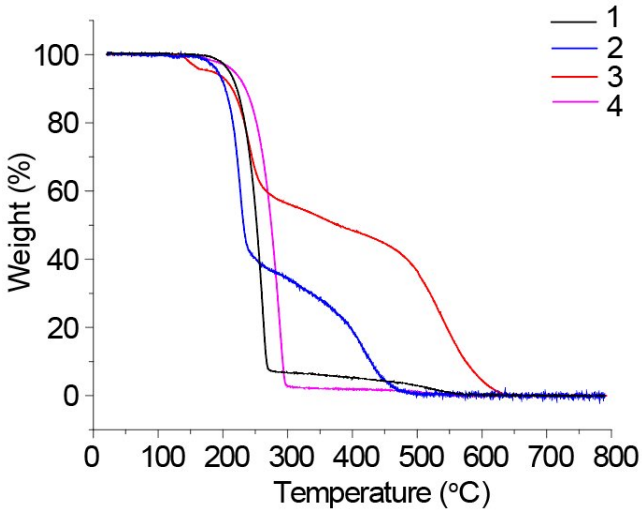

Figure S4. Thermogravimetric analysis (TGA) plots of compounds **1**-**4** measured at 20 °C/min showing the thermal stability of compounds **1**, **2**, and **4** up to 200 °C and that of compound **3** up to 180 °C.

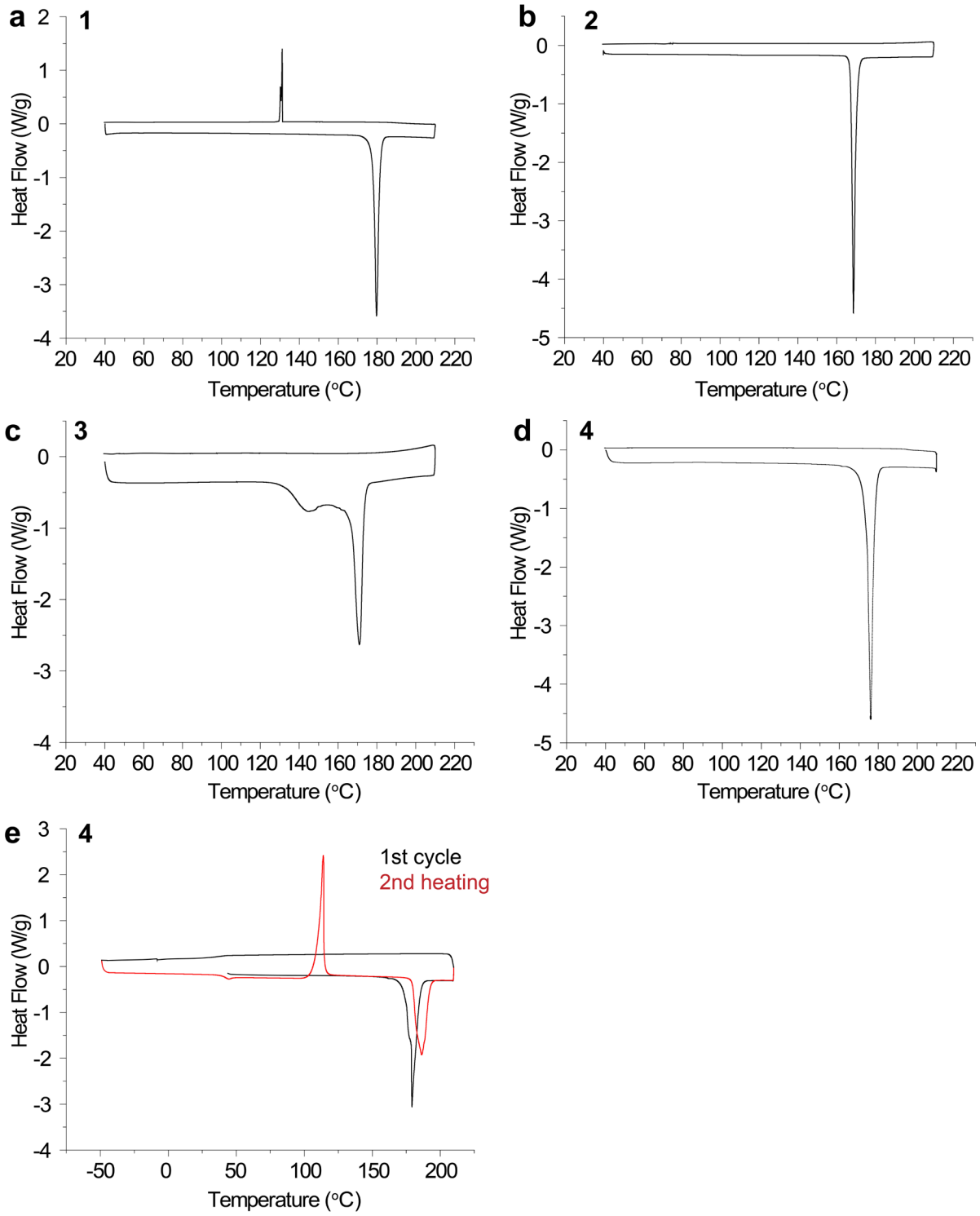

Figure S5. DSC plots of compound **1**-**4** (a-d) taken at a reduced cooling rate (2 °C/min). (e) DSC plot of compound **4** showing the sequential melting, supercooling, cold-crystallization, and re-melting (10 °C/min).

	1	2	3	4
T_m (°C)	180	169	171	179
T_c (°C)	122	-	-	-
T_g (°C)	-	54	58	44
T_{cc} (°C)	-	-	-	112
ΔH_m (J/g)	91.6	81.3	108.4	106.2
ΔH_c (J/g)	62.9	-	-	-
ΔH_{cc} (J/g)	-	-	-	64.4

Table S1. Thermodynamic parameters obtained by analyzing DSC cycles. T_m: melting point, T_c: crystallization point, T_g: glass transition point, T_{cc}: cold-crystallization point, ΔH_m: heat of fusion, ΔH_c: heat of crystallization, ΔH_{cc}: heat of cold-crystallization

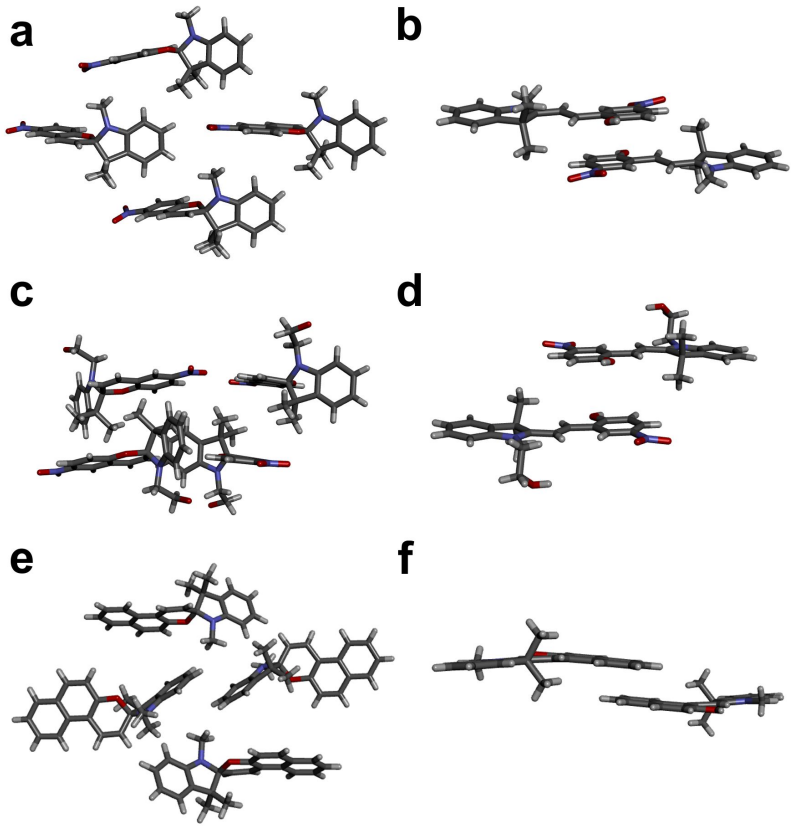

Figure S6. Reported crystal structures of spiropyran and merocyanine forms of compound **1** (a,b), **3** (c,d), and **4** (e,f).[5]

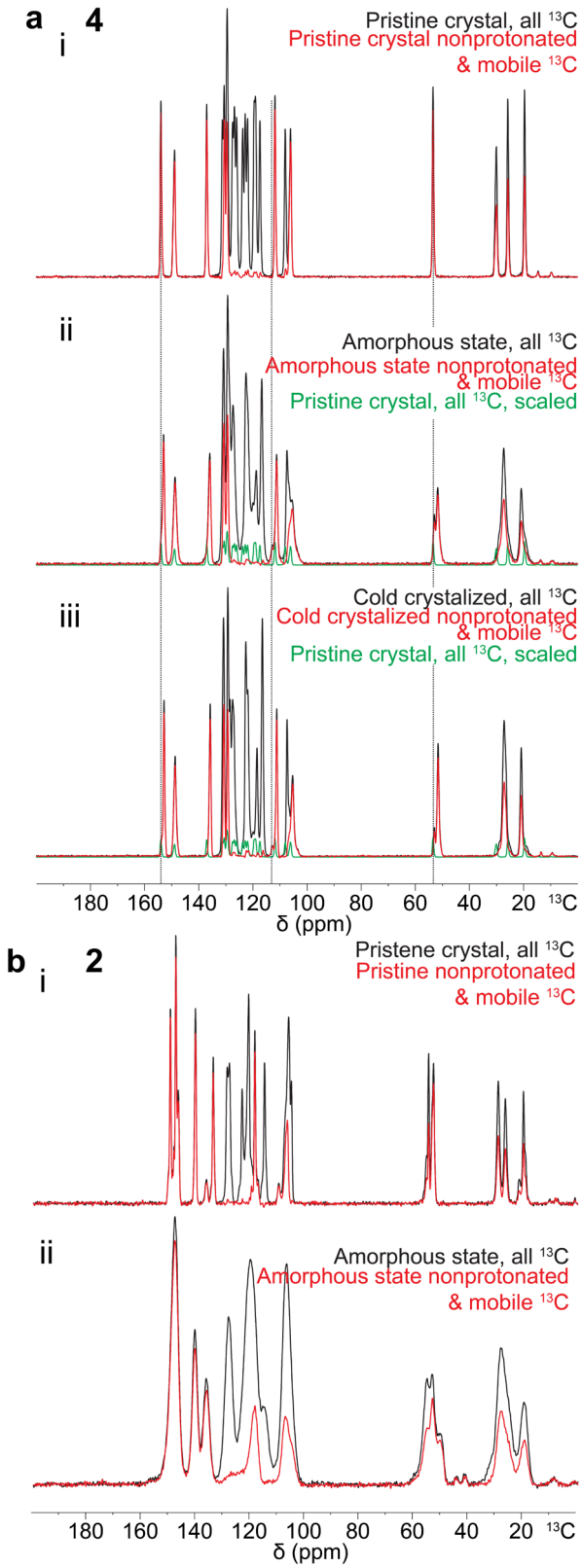

Figure S7. (a) Solid-state NMR spectra of compound **4**, showing (i) initial, (ii) after melting/cooling to room temperature, and (iii) cold-crystallized state. (b) Solid-state NMR spectra of compound **2**, showing (i) initial

state and (ii) state after melting/cooling to room temperature. Broadening of NMR peaks is observed for amorphous samples. The merocyanine content is negligible (<1 wt%) in all samples (measured at room temperature).

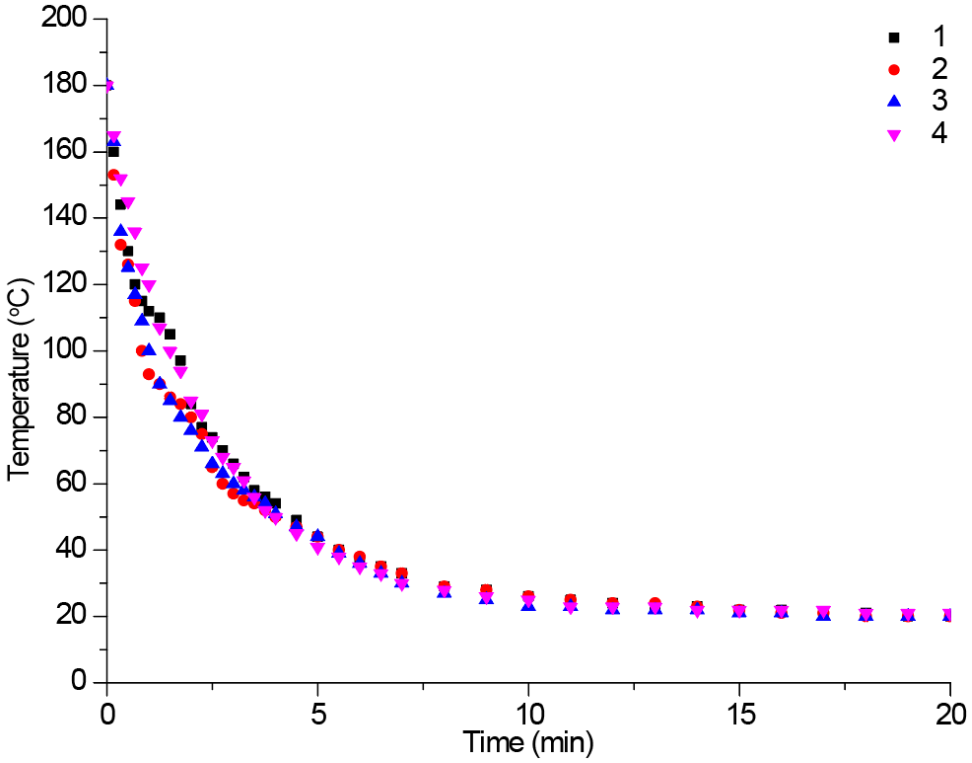

Figure S8. Temperature change of the films over time as cooled from the initial temperature of 180 °C.

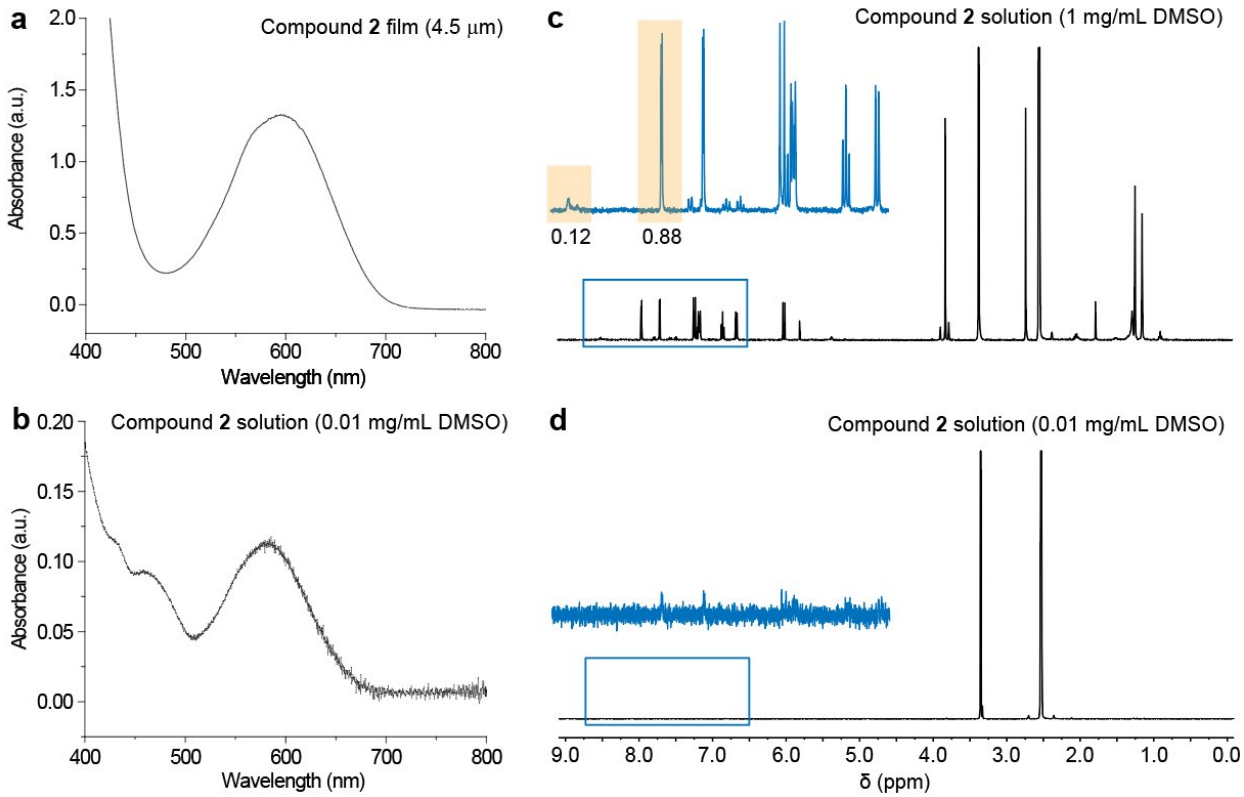

Figure S9. (a) UV-Vis spectrum of a film of compound **2**. (b) UV-Vis spectrum of compound **2** in DMSO (0.01 mg/ml). (c) ^{1}H NMR spectra of compound **2** in 1 mg/mL and (d) 0.01 mg/mL DMSO. The integration of peaks corresponding to MC and SP forms indicate 12:88 ratio of MC:SP in DMSO solutions. From the comparison of UV-Vis spectra (a) and (b), ~1 wt% of MC in SP film is calculated. We note that the detection of minor MC in identical solution (0.01 mg/mL) by UV-Vis was more facile than that by NMR, which has lower sensitivity than UV-Vis.

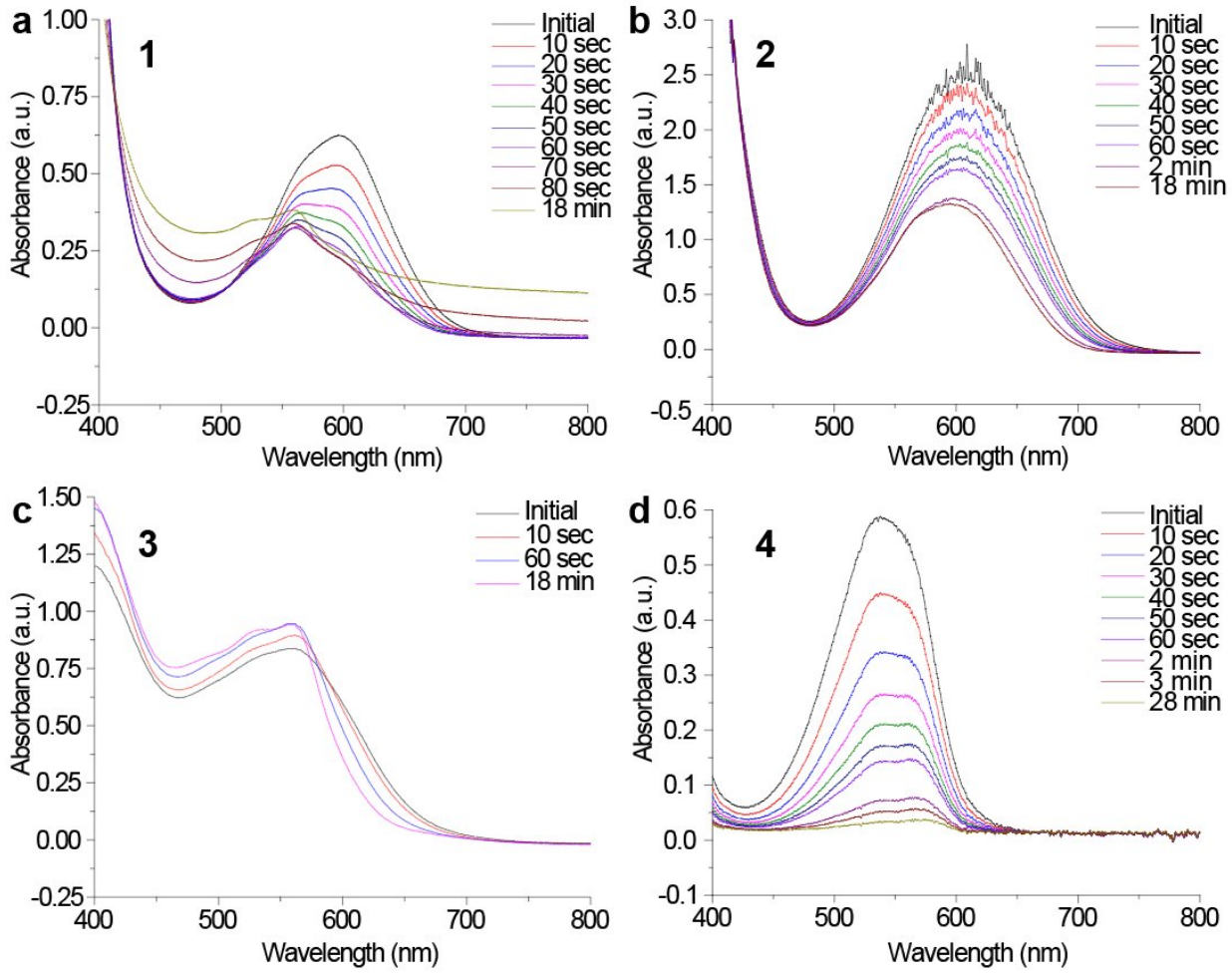

Figure S10. UV-Vis spectra of compounds **1**-**4** (a-d) in films cooled from 180 ^{o}C.

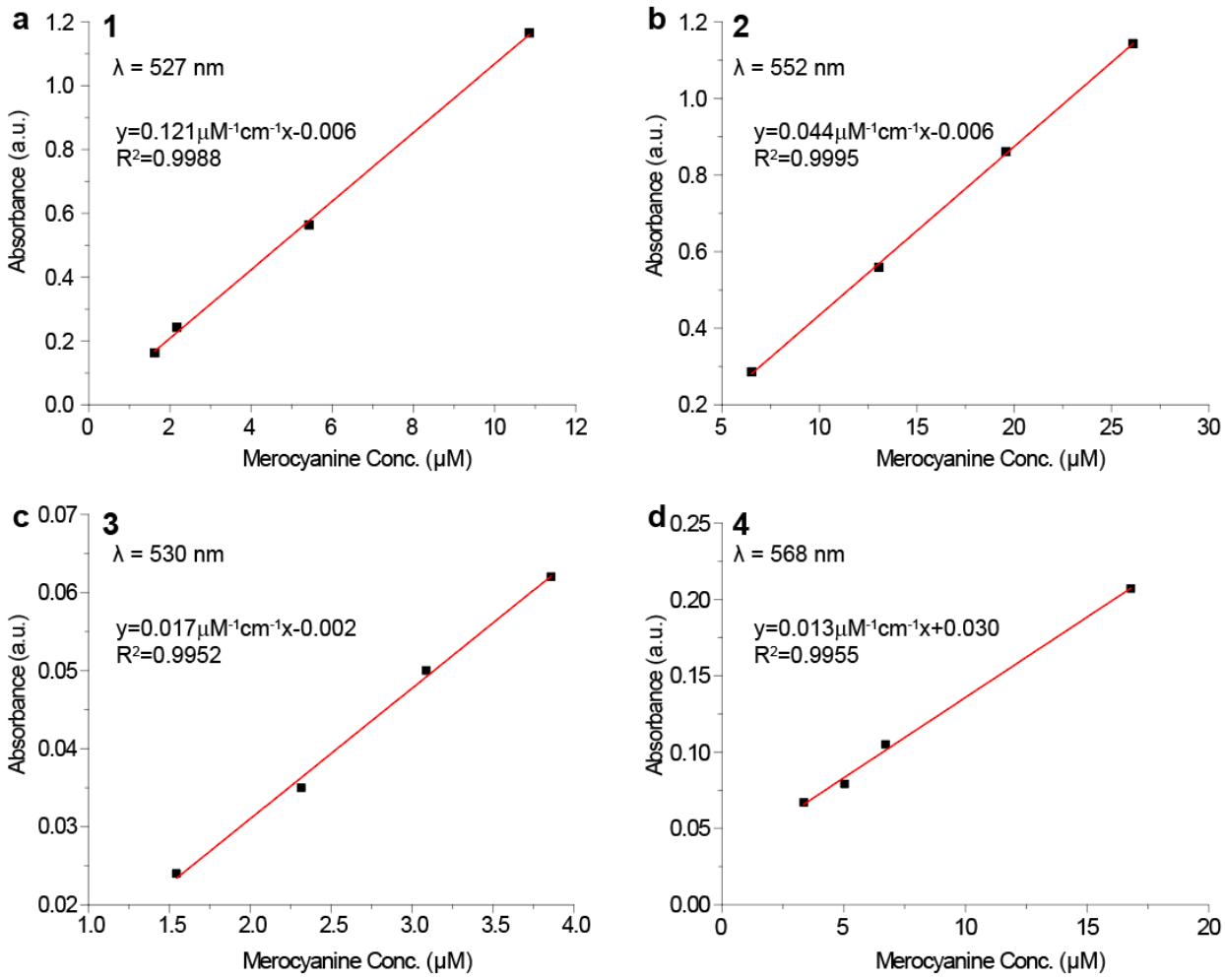

Figure S11. Molar extinction coefficient measurement of compounds **1**-**4** (a-d) in methanol.

	1	**2**	**3**	**4**
Thickness (μm)	5.0 ± 0.1	5.8 ± 0.3	1.1 ± 0.1	4.9 ± 0.1

Table S2. Film thickness of compounds **1**-**4** measured by a profilometer.

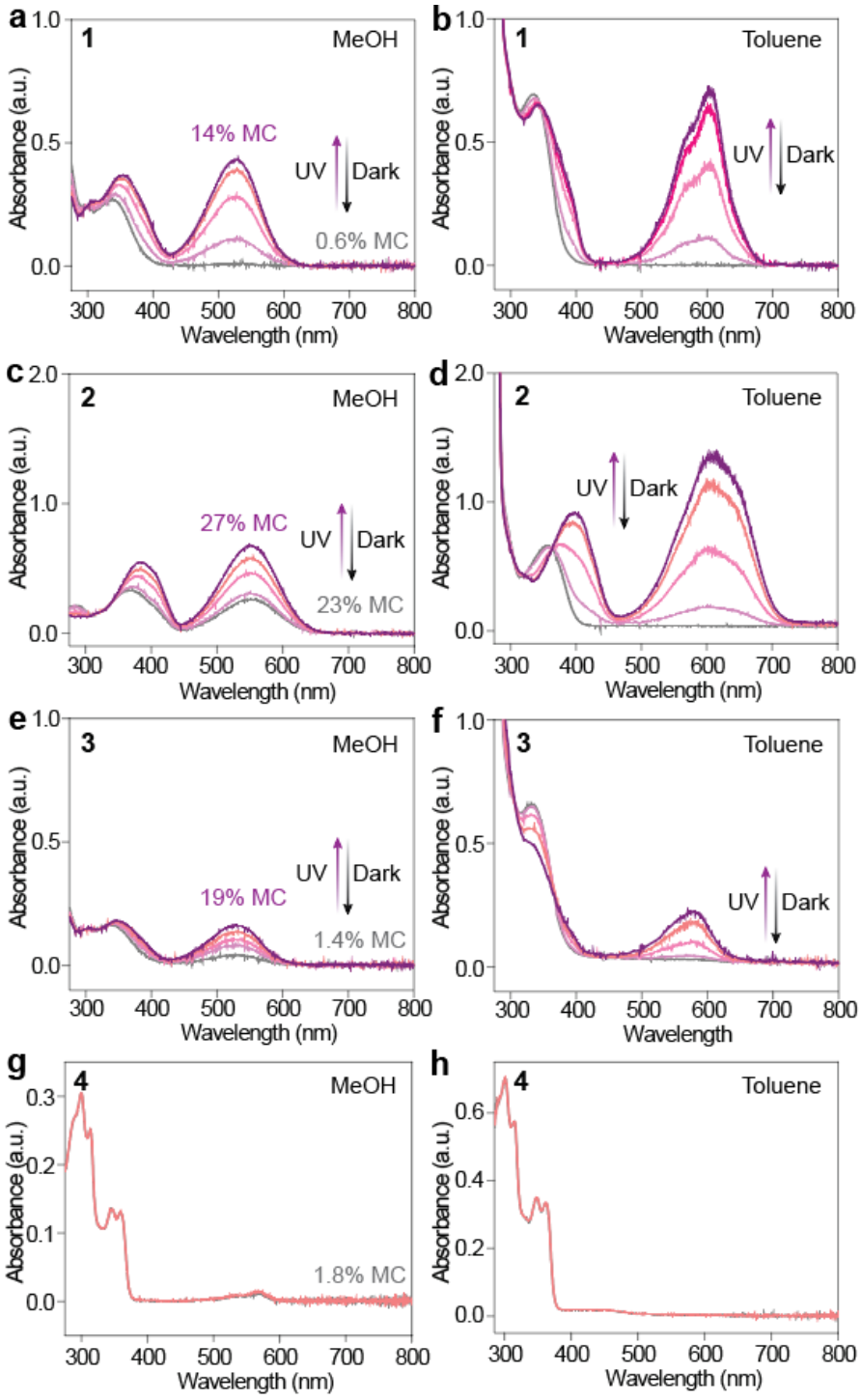

Figure S12. UV-Vis spectra of compounds **1**-**4** in methanol (a,c,e,g) and toluene solution (b,d,f,h) (10 µg/mL and 25 µg/mL respectively). As exposed to UV, SP isomerizes to MC, showing the increase of absorption peak in the visible region. The reversion of MC to SP occurs in the dark, accelerated in heated conditions. As compound **1**-**4** contains intrinsic mixture of MC and SP in methanol before UV-induced photo-

switching, we indicate the initial MC content in % by analyzing ^{1}H NMR as well as the final MC content in % after UV irradiation. Toluene solutions do not exhibit noticeable MC content before UV irradiation, and it was challenging to obtain ^{1}H NMR of the UV-charged toluene solution due to the fast reversion of MC to SP.

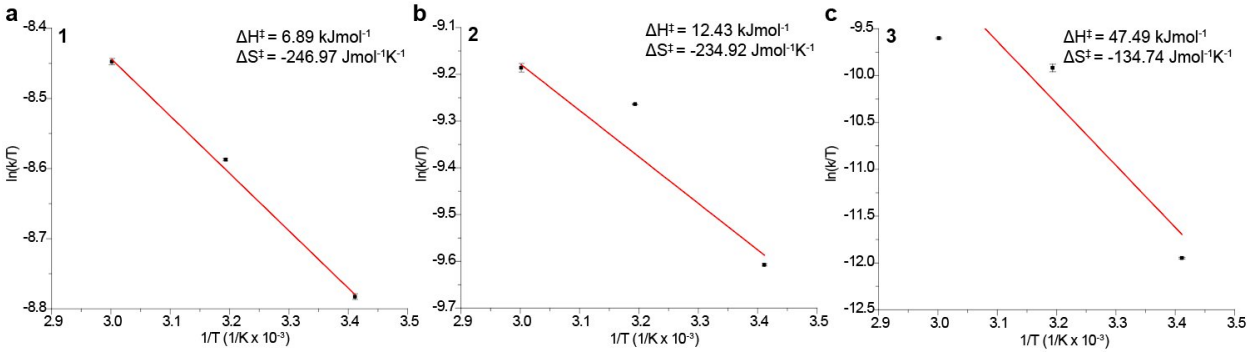

Figure S13. Eyring-Polanyi plots of compound **1**-**3**. The kinetic constants (k) were measured by analyzing the MC-to-SP reversion in toluene solutions (25 μg/mL) at 20 °C, 40 °C, and 60 °C right after saturating MC isomers by UV irradiation. $\Delta H^{‡}$ and $\Delta S^{‡}$ are shown in each plot. Error bars are present in each plot.

	1	**2**	**3**
k at 20 °C (sec^{-1})	0.045	0.020	0.002
k at 40 °C (sec^{-1})	0.058	0.027	0.015
k at 60 °C (sec^{-1})	0.071	0.034	0.023
$t_{1/2}$ at 20 °C (sec)	15.4	35.2	365
$t_{1/2}$ at 40 °C (sec)	11.9	23.3	44.9
$t_{1/2}$ at 60 °C (sec)	9.70	20.3	30.7

Table S3. k and $t_{1/2}$ measured for each solution at 20 °C, 40 °C, and 60 °C.

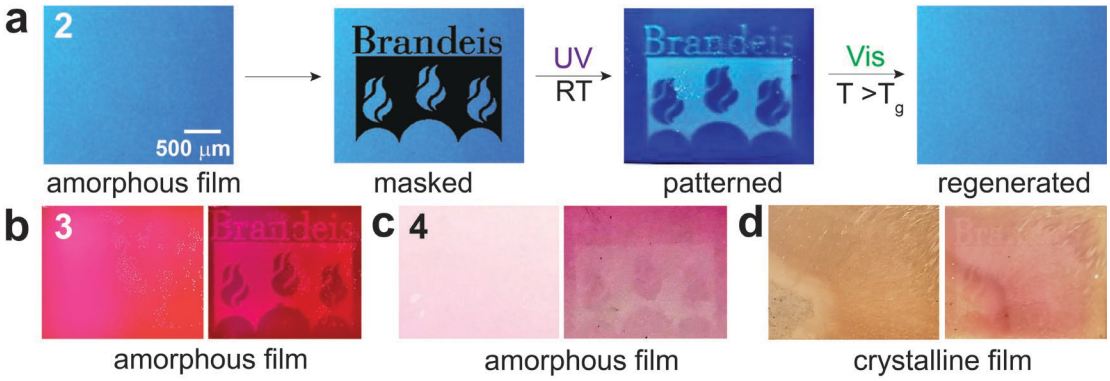

Figure S13. Thin film patterning experiment showing that exposure to UV effectively isomerizes SP molecules in the amorphous solid of compound (a) **2**, (b) **3**, and (c) **4**. (d) Crystalline film of compound **1** showing difficulty of patterning and crystalline features.

References

1 P. Duan and K. Schmidt-Rohr, *J. Magn. Reson*., 2017, **285**, 68-78.

2 B. M. Fung, A. K. Khitrin and K. Ermolaev, *J. Magn. Reson*., 2000, **142**, 97-101.

3 J. D. Mao and K. Schmidt-Rohr, *Environ. Sci. Technol*., 2004, **38**, 2680-2684.

4 W. T. Dixon, J. Schaefer, M. D. Sefcik, E. O. Stejskal and R. A. McKay, *J. Magn. Reson*., 1982, **49**, 341-345

5 (a) J. Harada, Y. Rawazoe, and K. Ogawa, *Chem. Commun*., 2010, **46**, 2593-2595; (b) F. M. Raymo, S. Giordani, A. J. P. White, and D. J. Williams, *J. Org. Chem*., 2003, **68**, 4158-4169; (c) W. Clegg, N. C. Norman, T. Flood, L. Sallans, W. S. Kwak, P. L. Kwiatkowski and J. G. Lasch, *Acta. Cryst. C.*, 1991, **47**, 817-824; (d) V. K. Seiler, K. Callebaut, K. Robeyns, N. Tumanov, J. Wouters, B. Champagne, and T. Leyssens, *CrystEngComm*, 2018, **20**, 3318-3327; (e) M. Colaço, A. Carletta, M. V. Gysel, K. Robeyns, N. Tumanov, and J. Wouters, *ChemistryOpen.,* 2018, **7**, 520-526.